A programmable bispecific nano-immuno-engager promotes T cell homing and reprograms tumour microenvironment

Lu Zhang
Department of Biochemistry and Molecular Medicine, UC Davis NCI-designated Comprehensive Cancer Center, University of California Davis

Ruonan Bo
Department of Biochemistry and Molecular Medicine, UC Davis NCI-designated Comprehensive Cancer Center, University of California Davis

Yi Wu
Department of Biochemistry and Molecular Medicine, UC Davis NCI-designated Comprehensive Cancer Center, University of California Davis

Longmeng Li
Department of Biochemistry and Molecular Medicine, UC Davis NCI-designated Comprehensive Cancer Center, University of California Davis

Zheng Zhu
Department of Biochemistry and Molecular Medicine, UC Davis NCI-designated Comprehensive Cancer Center, University of California Davis

Ai-Hong Ma
Department of Biochemistry and Molecular Medicine, UC Davis NCI-designated Comprehensive Cancer Center, University of California Davis

Wenwu Xiao
University of California, Davis

Yanyu Huang
Department of Biochemistry and Molecular Medicine, UC Davis NCI-designated Comprehensive Cancer Center, University of California Davis

Tatu Rojalin
Department of Biochemistry and Molecular Medicine, UC Davis NCI-designated Comprehensive Cancer Center, University of California Davis

Xingbin Yin
Department of Biochemistry and Molecular Medicine, UC Davis NCI-designated Comprehensive Cancer Center, University of California Davis

Yongheng Wang

Department of Biochemistry and Molecular Medicine, UC Davis NCI-designated Comprehensive Cancer Center, University of California Davis

Hongyong Zhang
Department of Biochemistry and Molecular Medicine, UC Davis NCI-designated Comprehensive Cancer Center, University of California Davis https://orcid.org/0000-0002-5669-5791

Kelmen Low
Department of Biochemistry and Molecular Medicine, UC Davis NCI-designated Comprehensive Cancer Center, University of California Davis https://orcid.org/0000-0001-5155-0158

Kiana Lee
Department of Biochemistry and Molecular Medicine, UC Davis NCI-designated Comprehensive Cancer Center, University of California Davis

Yousif Ajena
Department of Biochemistry and Molecular Medicine, UC Davis NCI-designated Comprehensive Cancer Center, University of California Davis

Di Jing
Department of Biochemistry and Molecular Medicine, UC Davis NCI-designated Comprehensive Cancer Center, University of California Davis

Dalin Zhang
Department of Biochemistry and Molecular Medicine, UC Davis NCI-designated Comprehensive Cancer Center, University of California Davis

Chris Baehr
Department of Biochemistry and Molecular Medicine, UC Davis NCI-designated Comprehensive Cancer Center, University of California Davis

Ruiwu Liu
UC Davis

Lei Wang
National Center for Nanoscience and Technology https://orcid.org/0000-0003-1405-9815

Yuanpei Li
Department of Biochemistry and Molecular Medicine, UC Davis NCI-designated Comprehensive Cancer Center, University of California Davis

Kit Lam (kslam@ucdavis.edu)
Department of Biochemistry and Molecular Medicine, UC Davis NCI-designated Comprehensive Cancer Center, University of California Davis https://orcid.org/0000-0002-3076-6969

Article

Keywords: Immune checkpoint blockade therapy, nano-immuno-engager, immunotherapeutics

Posted Date: November 15th, 2021

DOI: https://doi.org/10.21203/rs.3.rs-993445/v1

Abstract

Immune checkpoint blockade (ICB) therapy has revolutionized clinical oncology. However, the efficacy of ICB therapy is limited by the ineffective homing of T effector (T_{eff}) cells to tumours and the immunosuppressive tumour microenvironment (TME). Here, we report a programmable tumour cells/T_{eff} cells bispecific nano-immuno-engager (NIE) that can circumvent these limitations to improve ICB therapy. We have developed 28 nm non-toxic peptidic micellar nanoparticles (NIE-NPs) that bind $\alpha_3\beta_1$ integrin on tumour cells membrane and undergo *in situ* transformation on surface of tumour cells into nanofibrillar network (NIE-NFs). The nanofibrillar network persistently facilitates cytotoxic T cells' homing to the proximity of tumour cells *via* activatable $\alpha_4\beta_1$ integrin ligands, and also allows sustained release of resiquimod to reprogram the TME. This bispecific NIE eliminates syngeneic 4T1 breast cancer and Lewis lung cancer models in mice, when given together with anti-PD-1 antibody. The *in vivo* structural transformation-based supramolecular bispecific NIE represents an innovative class of programmable receptor-mediated targeted immunotherapeutics to greatly enhance ICB therapy against cancers.

Introduction

Immune checkpoint receptor pathway blockade monoclonal antibodies such as anti-PD-1, anti-PD-L1, and anti-CTLA-4 can reverse T effector (T_{eff}) cell dysfunction and exhaustion, resulting in dramatic tumour shrinkage and sometimes complete remission in some patients, even with late stage metastatic diseases.[1, 2] To date, the US Food and Drug Administration (FDA) had approved seven immune checkpoint blockade monoclonal antibodies (ICB-Ab): one CTLA-4 inhibitor (ipilimumab), three PD-1 inhibitors (nivolumab, pembrolizumab and cemiplimab), and three PD-L1 inhibitors (atezolizumab, durvalumab and avelumab), used either alone, or in combination with other therapies, against a range of tumour types.[3-5] However, the response rate varies greatly between tumour types: up to 40% in melanoma, 25% in non-small cell lung cancer, but <10% in most other tumour types.

The low response rate of ICB therapy was probably ascribed to defects in T_{eff} cell homing to the tumour sites.[6] In addition, tumour microenvironment (TME), comprised of immune and stromal cells, vasculature, extracellular matrix, cytokines, chemokines, and growth factors, can all influence tumour response to ICB therapies. Other mechanisms of ICB resistance include the presence of regulatory T (T_{reg}) cells, myeloid-derived suppressor cells (MDSCs), and M2 tumour-associated macrophages (TAMs) at the immunosuppressive TME.[7] Elevated level of CCL5, CCL17, CCL22, CXCL8 and CXCL12 facilitates the recruitment of T_{regs} and MDSCs to the TME, resulting in a diminished ICB response. In contrast, CXCL9 and CXCL10 promote homing of cytotoxic T-cells to the tumour sites, boosting anti-tumour immune response; transforming growth factor beta (TGF-b) does the opposite and upregulates T_{regs}. Oncogenic or tumour suppressor pathways, such as mitogen-activated protein kinase (MAPK) and PI3K-g in the cancer cells can also influence TME by altering the immune cell compositions and cytokine profile. Toll-like receptors (TLRs) 7/8 agonists have been shown to be able to reprogram the TME and enhance the function of immune cells.[8, 9]

In an attempt to overcome ICB resistance, many combination therapeutic strategies have been tried preclinically and clinically.[7] These include the addition of the following drugs to a ICB-Ab: one other ICB-Ab (antibodies against CTLA-4, PD-1, PD-L1, LAG-3 and TIM-3), chemotherapeutic agents (paclitaxel, gemcitabine and carboplatin), radiation therapy, targeted therapy (inhibitors against PI3K, VEGF, BRAF/MEK, IDO, A2AR, FGFR, EGFR, PARP and mTOR), macrophage inhibitors (inhibitors against CSF1R and ARG1), cytokine/chemokine inhibitors (inhibitors against CXCR4, CXCR2 and TGF-b), epigenetic modulators (histone deacetylase inhibitors and hypomethylating agents), immunomodulatory agents (antibodies against OX40, 41BB, GITR, CD40 and ICOS), adoptive cell transfer therapy (car T, TIL and TCR), and modulation of gut microbiome. The development of a therapeutic modality that can reliably alter the complex tumour immune microenvironment favoring tumour regression is a big challenge, preclinically and clinically.

Advancement and optimization of nano-immunotherapy lie in the development of innovative approaches to enhance the specificity and controllability of immunotherapeutic interventions, and the targeting of desired cell types. Advanced bionanomaterials or approaches in a more controlled manner could enhance immunotherapeutic potency by increasing the accumulation and prolonging the retention of immunomodulatory and immune cell homing agents at the TME while sparing the normal tissues and organs, thus reducing off-target adverse effects such as systemic cytokine storm.[10-15] Especially, *in situ* modulation of nanomaterial *in vivo* has been demonstrated to improve the performance of bioactive molecules.[16-21]

In order to improve ICB therapy, here we report on a programmable tumour cells/T_{eff} cells bispecific nano-immuno-engager (NIE) that can enhance the homing of T_{eff} cells to the tumour sites and sustainably release immunoagonist to reprogram the TME. This bispecific NIE, initially in nanoparticle form (NIE-NPs), is self-assembled from two transformable peptide monomers (TPMs, Fig. 1a). TPM1, LXY30-KLVFFK(*Pa*), was comprised of three discrete functional domains: (1) the high-affinity and high-specificity LXY30 cyclic peptide (cdG-Phe(3,5-diF)-G-Hyp-NcR) ligand that targets $\alpha_3\beta_1$ integrin heterodimeric transmembrane receptor expressed by many epithelial tumours,[22] (2) the KLVFF b-sheet forming peptide domain originated from β-amyloid (Aβ) peptide,[16, 23-25] and (3) the pheophorbide a (*Pa*) moiety with fluorescence property, serving as a hydrophobic core to induce the formation of micellar nanoparticles. TPM2, *pro*LLP2A-KLVFFK(*R848*), was also comprised of three discrete functional domains: (1) *pro*LLP2A, the “pro-ligand” version of LLP2A ligand that is a high-affinity and high-specificity peptidomimetic ligand against activated $\alpha_4\beta_1$ integrin of lymphocytes,[26] (2) the same KLVFF b-sheet forming peptide domain, and (3) R848 (resiquimod), a hydrophobic TLRs 7/8 agonist, grafted to TPM2 main chain *via* an ester-bond. In *pro*LLP2A, the carboxyl group of LLP2A is blocked by 3-methoxy-1-propanol through esterification such that it will not interact with normal lymphocytes and mesenchymal stem cells during blood circulation.

Under aqueous condition and in blood circulation, TPM1 and TPM2, at a ratio of 1:1, would co-self-assemble into nanoparticles, NIE-NP, in which KLVFFK(Pa) and KLVFFK(R848) hydrophobic domains were

in the interior of the NIE-NPs, while relatively hydrophilic LXY30 and *pro*LLP2A ligand peptides were on the surface of the NIE-NPs. NIE-NPs would be preferentially taken up by tumours through the leaky tumour vasculatures (enhanced permeability retention effects). Upon interaction with $\alpha_3\beta_1$ integrin receptor protein displayed on the tumour cell membrane, the NIE-NPs would undergo *in situ* transformation into nanofibrillar structural network (NIE-NFs) on the surface of tumour cells, thus maintaining a prolonged retention of the nanofibrillar network of NIE at the tumour sites (at least 7 days). With the abundant esterase in the TME and on the tumour cells, *pro*LLP2A would quickly be converted to LLP2A (T cell ligand) against activated a_4b_1 integrin. LLP2A displayed on the fibrils would facilitate the homing and retention of T_{eff} cells (e.g. $CD8^+$ T cells) at the TME and adjacent to the tumour cells. The homing and retention of large numbers of T_{eff} cells would greatly enhance ICB therapy. Anti-PD-1 antibody would greatly activate the NIE homed cytotoxic T cells for ICB therapy.[15, 27-29] Besides, the sustained release of R848 from the nanofibrillar network would improve immunosuppressive tumour microenvironment, e.g., activate antigen-presenting cells, promote immune cells to produce anti-tumour response factors, and re-educate the phenotype of macrophage from M2 to M1.[8] This *in vivo* structural transformation-based supramolecular bispecific NIE represents an innovative class of programmable receptor-mediated targeted immunotherapeutics against cancers *via* enhancing T cell homing to the tumours and improving the TME (Scheme 1).

Results

Self-assembly, fibrillar transformation and esterase hydrolysis of programmable bispecific NIE

Two transformable peptide monomers (TPM1 and TPM2) were synthesized and characterized (Fig. 1a and Supplementary Fig. 1). As the proportion of water in the mixed solvent (water and DMSO) of the TPM1 and TPM2 mixture solution (the ratio of 1:1) was increased, there was a gradual decrease in fluorescence peak at 675 nm due to the aggregation-caused quenching (ACQ) properties of *Pa* dye (Fig. 1b), reflecting the gradual formation of NIE-NPs *via* self-assembly. Concomitantly, there was a modest decrease in the absorption peak at both 405 and 680 nm (Supplementary Fig. 2a). Nanoparticles were analyzed by transmission electron microscopy (TEM) and dynamic light scattering (DLS). TPM1 and TPM2 each alone were able to self-assemble to form nanoparticles (NPs_{TPM1} and NPs_{TPM2}) at 18 and 55 nm, respectively. NIE-NPs, assembled from 1:1 mix of TPM1 and TPM2 into nanoparticles at around 28 nm, which fell between the sizes of NPs_{TPM1} and NPs_{TPM2} (Supplementary Fig. 2b). The critical aggregation concentration (CAC) of NIE-NPs was determined to be 8 μM (Supplementary Fig. 2c). We have also demonstrated that NIE-NPs could maintain good serum stability and proteolytic stability over 7 days at 37 ^oC (Supplementary Fig. 2d).

To verify the receptor-mediated fibrillar transformable process of NIE-NPs *in vitro*, soluble $\alpha_3\beta_1$ integrin protein (receptor for LXY30) was added to NIE-NPs solution. After 24 h of incubation at room temperature, a fibrillar network (NIE-NFs, width diameter about 8 nm) with a broad size distribution was clearly detected (Fig. 1c,f). No transformation was observed in the NIE-NPs preparation without the

addition of $\alpha_3\beta_1$ integrin protein, even after 24 h (Supplementary Fig. 2e). The CAC of NIE-NFs was determined to be 5 μM, which was lower than that of NIE-NPs (8 μM), indicating that NIE-NFs has higher propensity to form nanostructures than NIE-NPs (Supplementary Fig. 2f). The process of NIE-NPs transformation could be monitored by the fluorescent intensity of *Pa* (Fig. 1d). Addition of $\alpha_3\beta_1$ integrin protein triggered a gradual decrease in fluorescence intensity of *Pa* over time, reflecting an increase in fluorescence quenching in NFs1, indicating that the packing of *Pa* in NIE-NFs was denser. In addition, a 5 nm fluorescence red shift (from 675 nm to 680 nm) with fluorescence peak reversal (from 680 nm to 725 nm) were observed, indicating that the disordered arrangement of *Pa* in the core of NIE-NPs was transformed into J-aggregate form in NIE-NFs.[30-32] We have also investigated the responsiveness of *pro*LLP2A displayed on the NIE-NPs surface to soluble $\alpha_4\beta_1$ integrin protein in the presence and absence of esterase (Fig. 1e,f and Supplementary Fig. 3). Soluble $\alpha_4\beta_1$ integrin protein alone was not able to alter the structure of NIE-NPs displaying *pro*LLP2A, even after 24 h of incubation. In contrast, successive addition of esterase, followed by soluble $\alpha_4\beta_1$ integrin protein was able to elicit conversion of NIE-NPs to fibrillar network after 24 h of incubation. This expected result confirmed that esterase was able to convert pro-ligand *pro*LLP2A to ligand LLP2A, which in turn was able to trigger receptor-mediated transformation of NIE-NPs to NIE-NFs. We also monitored the conversion of *pro*LLP2A ligand to LLP2A ligand by HPLC. As shown in Supplementary Fig. 4, majority of *pro*LLP2A were found to be converted to LLP2A after incubation with porcine liver esterase for 8 h at pH 7.4 and 37 ^{o}C.

Circular dichroism (CD) spectroscopic analysis of the transformation process of NIE-NPs showed a gradual progression of a negative signal at 216 nm and a positive signal at 195 nm upon incubation with $\alpha_3\beta_1$ integrin protein or combination esterase/$\alpha_4\beta_1$ integrin protein, indicative of β-sheet formation (Fig. 1g) and consistent with TEM results shown in Fig. 1c,e.[23, 33] *In vitro* release behaviour of R848 from NIE-NFs was studied at pH 6.5 with addition of esterase to simulate TME condition. As shown in Fig. 1h, about 45% of R848 was released in the first 24 h, after which the release rate gradually slowed down and about 86% cumulative release was observed by 168 h, indicating that prolonged and sustained release of R848 could occur at the TME, which may be due to the slow hydrolysis of the ester bond to R848 within the fibrillar structure. To demonstrate the unique transformable property of NIE-NPs, we designed a related negative control nano-immuno-engager nanoparticle (CNIE-NP) formed by assembly of two negative control TPMs without b-sheet forming KLVFF peptide sequence, at a ratio of 1:1 (CTPM3: LXY30-KAAGGK(*Pa*) and CTPM4: *pro*LLP2A-KAAGGK(*R848*), Supplementary Fig. 1). As expected, $\alpha_3\beta_1$ integrin protein was unable to transform CNIE-NPs to fibrillar structures even after 24 h, indicating that the b-sheet peptide was required for the transformation of NIE-NPs to NIE-NFs (Supplementary Fig. 5a,b). CD spectroscopic analysis of CNIE-NPs remained the same with or without the addition of $\alpha_3\beta_1$ integrin protein, indicating that β-sheet was not formed (Supplementary Fig. 5c).

In vitro evaluation of bispecific NIE facilitating T_{eff} cells homing and reeducating macrophages

We investigated the binding affinity and selectivity of LXY30 to a_3b_1 integrin and LLP2A to a_4b_1 integrin *via* flow cytometry. To ensure the specificity and accuracy of binding analysis, K562 human myeloid

leukemia cell line stably transfected with a_3b_1 or a_4b_1 integrins were used. As shown in Supplementary Fig. 6a, biotinylated LXY30 ligand displayed little affinity for K562 (a_4b_1+) cells, whereas biotinylated LLP2A ligand showed high affinity for these cells. As expected, *pro*LLP2A ligand showed no significant affinity to these a_4b_1 integrin expressing cells, but the affinity was restored after *pro*LLP2A ligand was treated with esterase (Supplementary Fig. 6b). We also analyzed the binding affinity of LXY30 and LLP2A ligand to K562 (a_3b_1+) cells. As shown in Supplementary Fig. 6c, LXY30, but not LLP2A, was found to have high affinity against these a_3b_1 integrins expressing cells. To further characterize the interaction between NIE-NPs and $\alpha_3\beta_1$ integrin receptors on the surface of living cells, we chose $\alpha_3\beta_1$ integrin expressing 4T1 murine breast cancer cell. As expected, flow cytometry analysis confirmed that LXY30, the high affinity $\alpha_3\beta_1$ integrin ligand, did bind to 4T1 tumour cells (Supplementary Fig. 7). We have also found that NIE-NPs was slightly cytotoxic against 4T1 tumour cells, with 84.5% cell viability at 50 mM (Supplementary Fig. 8). We investigated the distribution of nanoparticles by tracking the red fluorescent signal emitted by *Pa* using confocal laser scanning microscopy (CLSM). Six hours after incubation of 4T1 tumour cells with NIE-NPs, a strong red fluorescence signal was observed on the cell surface and its vicinity but not inside the cells (Fig. 2a). In contrast, the fluorescent signal of *Pa* in CNIE-NPs-treated group was found to be concentrated primarily in the cytoplasm of the cells. To study the retention and stability of formed nanofibrillar network on the surface of tumour cells, unbound nanoparticles were washed off after 6 h of incubation and fresh medium without nanoparticles was added to incubate cells for another 18 h. As expected, NIE-NPs treated cells still retained strong red fluorescence signals on the cell surface at 24 h, displaying that the capacity of prolonged retention of bispecific NIE (Fig. 2b). In sharp contrast, only weak fluorescence signal was observed inside the cells treated with CNIE-NPs after 24 h. This is probably due to the enzymatic degradation of the already endocytosed CNIE-NPs after 18 h of incubation, but without any new endocytic uptake during that time period. TEM images confirmed the presence of nanofibrillar network on the surface of, and between 4T1 tumour cells after incubation with NIE-NPs for 24 h, but absence of such nanofibrillar structures on cells treated with CNIE-NPs (Fig. 2c). The fibrillar structures further away from the tumour cell surface were probably induced by the secreted tumour exosomes displaying $\alpha_3\beta_1$ integrin proteins.[16, 34] We also investigated the effect of esterase on the interactions between NIE-NPs and T-cell surface a_4b_1 integrin, after converting pro-ligand *pro*-LLP2A to LLP2A displayed on the surface of NIE-NPs. Live GFP transfected Jurkat T-lymphoid leukemia cells with high expression level of constitutively activated a_4b_1 integrin protein were used to mimic T cells. As shown in Fig. 2d, after 6 h incubation of Jurkat cells with NIE-NPs (pre-treated with esterase), a luxuriant red fluorescent layer was found surrounding the Jurkat cells, indicating that the conversion of pro-ligand to LLP2A ligand was successful. Scanning electron microscopy (SEM) confirmed the presence of fibrillar network on the surface of NIE-NPs-treated 4T1 tumour cells and esterase pre-treated NIE-NPs-treated Jurkat cells (Fig. 2e).

To simulate the processes of initial fibrillar transformation of NIE-NPs on the 4T1 tumour cells surface followed by T cell homing, we incubated 4T1 tumour cells with NIE-NPs for 6 h, unbound NIE-NPs were then washed off, followed by addition of fresh medium containing esterase but without NIE-NPs. After 1 h

of incubation, Jurkat cells were added and incubated with 4T1 tumour cells for 2 or 4 h. After that, unbound Jurkat cells were gently removed prior to CLSM imaging (Fig. 2f). As expected, a fibrillar structure layer with red fluorescence was detected surrounding 4T1 tumour cells surface, and Jurkat cells (GFP+) were found to interact with the red fluorescent fibrillar network (bispecific NIE) and in close proximity to 4T1 tumour cells, after 2 h of incubation. As the incubation time was increased to 4 h, many more Jurkat cells were found around the 4T1 tumour cells, which was consistent with our notion that nanofibrillar-based bispecific NIE would facilitate the homing of immune cells. SEM imaging provided critical evidence that the bispecific NIE had played a significant role in direct physical contact between 4T1 tumour cells and Jurkat cells through nanofibrillar network (Fig. 2g). In addition to using Jurkat cells as the surrogate T-cells, we also examined the effects of NIE on the killing of 4T1 tumour cells by activated murine CD8 T cells (a_4b_1 integrins pre-activated by Mn^{2+}). As shown in Supplementary Fig. 9, NIE-NP transformed into nanofibrillar network on the tumour cell surface, and as a result of esterase treatment, the displayed LLP2A captured activated T-cells, leading to about 50% tumour cell kill (Supplementary Fig. 10), confirming that the nanofibrillar network did not dampen immune synapse formation and killing efficiency of CD8 T cells. Similar studies were also performed on the negative control CNIE-NPs, which were taken up by 4T1 tumour cells, instead of forming nanofibrillar network on the cell surface, and as expected, no bound Jurkat cells were detected (Supplementary Fig. 11).

The conversion of TAMs from an immunosuppressive M2-polarized phenotype to an anti-tumourigenic M1-polarized phenotype is one of the major immunotherapeutic strategies for reprograming the immunosuppressive TME. Macrophage polarization states demonstrate hallmark morphology, e.g., elongated projections for M2-like cells as opposed to a round and flattened morphology for M1-like cells (Supplementary Fig. 12). IL-4 has been used to induce bone marrow derived macrophages (BMDM) to M2-polarized macrophages, as reflected by the increase in expression level of the metabolic checkpoint enzyme arginase-1 (Arg1) and mannose receptor-1 (Mrc1). R848 has been reported to be a powerful driver of the M1-phenotypes *in vitro*, resulting in elevated level of interleukin 12 (IL-12) and nitric oxide synthase (Nos2) produced by these cells.[8] Here we investigated the possibility of using NIE-NFs to reeducate macrophages from M2 phenotype to M1 phenotype. Not unexpected, incubation of M2-state macrophages with NIE-NFs, preformed from NIE-NPs with soluble a_3b_1 integrin protein, did not have significant change in morphology and expression level of Arg1 and Mrc1 even after 12 h (Fig. 2h), which can be explained by the lack of R848 released from NIE-NFs. In contrast, addition of esterase to the culture medium followed by 12 h incubation resulted in morphological change of M2-state macrophages towards M1-state, a decrease in Arg1 and Mrc1, and an increase in IL-12 and Nos2 expression as measured by qPCR. These changes were even more pronounced after 24 h, at which time the macrophages were completely transformed to a round and flattened morphology, with further decrease in Arg1 and Mrc1, and increase in IL-12 and Nos2 expression. We believe the ability of bispecific NIE to anchor on the surface of tumour cells, affording the sustained release of R848 from the fibrillar network, would generate a durable anti-cancer immunoactive TME. Interestingly, we have also found a significant change in macrophage morphology from M2-state towards M1-state after 24 h treatment with CNIE-NPs, which was perhaps because the particulate CNIE-NPs were phagocytosed by M2-macrophages, releasing

R848 intracellularly, resulting in conversion of these macrophages from M2 to M1 phenotype (Supplementary Fig. 13).

In vivo evaluation of bispecific NIE targeting tumour cells and nanofibrillar-transformation to facilitate T_{eff} cell homing and activate immunity

NIE-NPs was found to be non-toxic: blood counts, platelets, creatinine and liver function tests obtained from normal Balb/c mice treated with eight consecutive q.o.d. intravenous (i.v.) doses of NIE-NPs (13 mg/kg) were within normal limits (Supplementary Figs. 14 and 15). *In vivo* blood pharmacokinetics (PK) studies in rats showed that NIE-NPs possessed a long circulation time (T-half (α): 2.866 h and T-half (β): 23.186 h), indicating its stability during circulation (Supplementary Fig. 16). For biodistribution studies, NIE-NPs were tail vein injected once (13 mg/kg) into Balb/c mice bearing syngeneic orthotopic 4T1 breast cancer; 10, 24, 48, 72, 120 and 168 h later, tumour and main organs were excised for *ex vivo* fluorescent imaging (Fig. 3a,b). Significant fluorescent signal of *Pa* was found to persist in tumour tissue for over 168 h, while fluorescent signal in normal organs began to decline after 10 h and was almost undetectable in the main organs at 72 h. In sharp contrast, fluorescent signal of *Pa* at tumour tissue treated by CNIE-NPs was found to gradually decline over time after peaking at 24 h (Fig. 3c). By 168 h, less than 2.91% of the peak fluorescent signal for CNIE-NPs remained in the tumour, whereas for NIE-NPs, over 60.49% signal remained in the tumour (Fig. 3d). We also found that the red fluorescence signals from pheophorbide a (*Pa*) in NIE-NPs were detected throughout the entire tumour tissue, not just in the tumour periphery (Supplementary Fig. 17). Most of the red fluorescence (*Pa*) was observed in the extracellular space in close proximity to the tumour cell membranes, as indicated by the green arrows. Prolonged retention of fluorescent signal in NIE-NPs-treated mice could be attributed to *in situ* receptor-mediated transformation of NIE-NPs into NIE-NFs at the TME. TEM studies on excised tumour sections, 72 h after i.v. administration, showed abundant bundles of nanofibrils in the extracellular matrix while no such nanofibrils were observed in negative CNIE-NPs-treated and untreated mice (Fig. 3e). Fluorescent micrographs of tumour and overlying skin revealed intense fluorescent signal in tumour region but negligible signal in normal skin (Fig. 3f). This is consistent with our notion that (1) NIE-NPs would leak into the TME through leaky tumour vasculatures (EPR effect), followed by interaction with a_3b_1 integrin on tumour cells and tumour associated exosomes to generate NIE-NFs, and (2) blood vessels are not leaky in normal skin. The tumour tissue distribution of R848 over time was also determined with high pressure liquid chromatography-mass spectroscopy (HPLC-MS, Fig. 3g). We found R848 uptake by tumour was quite high at 24 h (3.62 μg per g tissue), and about one-third of R848 was found to retain at the tumour site (1.14 μg per g tissue) even at 7 days after injection of NIE-NPs. Although CNIE-NPs could also deliver significant amount of R848 to the tumour site (83% of what NIE-NPs could deliver), retention of R848 at the tumour site was much lower than that of NIE-NPs. Prolonged retention and release of R848 in tumour site indicates that a sustained immune-active TME could be achieved with NIE.

To evaluate if the bispecific NIE displaying LLP2A and R848 at the TME could facilitate T_{eff} cells homing to the tumour sites and reeducate TAMs *in vivo*, tumours from NIE-NPs-treated mice were excised on day 15 after a single i.v. injection of NIE-NPs (13 mg/kg), and the immune cell populations within the

tumours were analyzed by flow cytometry, immunohistochemistry (IHC) and qPCR. Experiment using CNIE-NPs as an untransformable/endocytic negative control group was also performed at the same time. We found that tail-vein injection of NIE-NPs resulted in greatly increase concentration ratio of cytotoxic T cells and a sustained immunoactive TME. First, NIE-NPs was found to significantly stimulate the production of chemokine CXCL10 at the tumour site (Fig. 3h), which was known to facilitate T_{eff} cells recruitment.[35, 36] This should be attributed to R848 which is known to induce the production of chemokines.[37, 38] R848 covalently linked to NIE-NPs *via* an ester bond was released from the nanofibrillar network anchored at the TME by endogenous esterases. As a result, released R848 would interact with a variety of cells in the TME, such as tumour cells, endothelial cells, and some immune cell subsets (dendritic cells, monocytes, macrophages, and B cells) to produce a range of chemokines and cytokines. Indeed, we observed that the proportion of $CD45^+CD3^+$ and $CD45^+CD3^+CD8^+$ T cells in the NIE-NPs-treated tumour tissue was substantially higher than those from mice treated with endocytic CNIE-NPs or saline (Fig. 3i, Supplementary Fig. 18 and 19a). More specifically, the percentage of $CD3^+CD8^+$ T effector cells in tumours was found to be 18 and 4-fold increase, relative to that of saline and CNIE-NPs-treated mice, respectively.

Second, we found that the relative abundance of $CD4^+Foxp3^+$ T_{regs} at the tumour site was substantially lower in mice that received NIE-NPs treatment than those in mice treated with CNIE-NPs, i.e. (4.97% versus 13.0%) or saline (4.97% versus 14.6%). The ratio of tumour-infiltrating $CD8^+$ killer T cells to immunosuppressive T_{regs} ($CD3^+CD4^+Foxp3^+$), which could be an indicator of anti-tumour immune balance, was found to be the highest in NIE-NPs treated group. We also analyzed the expression ($CD49^+$) and activation ($CD29^+$) of a_4b_1 integrin in tumour-infiltrating and blood circulating CD8 and CD4 T cells (Fig. 3i and Supplementary Fig. 19b,c). Although both blood circulating and tumour infiltrating CD8 and CD4 T cells in mice bearing 4T1 tumour were found to be both CD49+ and CD29+, their expression levels were higher in the tumour infiltrating cell populations. This may be because there was more chemokine and cytokine secretion in tumour tissues, therefore inducing more a_4b_1 integrin expression and activation. More excitingly, we found that after NIE-NPs treatment, there were more $CD8^+CD49^+$ T cells and $CD8^+CD29^+$ T cells in both circulating and tumour infiltrating cell populations. This data indicates that NIE-NP treatment, probably *via* chemokine induction, could promote CD49 expression and CD29 activation of T cells, and therefore homing and retention of these cells by the displayed LLP2A at the TME. We also evaluated T cell activation and exhaustion makers (CD69 and LAG-3) in tumour tissues, which could better access the killing effect of T cells against 4T1 tumour cells (Supplementary Fig. 20). Compared to CNIE-NPs and saline treated groups, mice treated with NIE-NPs exhibited higher CD69 expression and lower LAG-3 (an immune check point receptor) expression, the desirable anti-tumour immune phenotype of the TME. IHC staining of tumour tissue sections also confirmed an increase in CD8/CD4 and decrease in Foxp3 positive T_{reg} cells (Fig. 3j).

Third, IHC staining of tumour sections demonstrated an increase in M1-polarized macrophage marker CD68 and a decrease in M2-polarized macrophage marker CD163 in the NIE-NPs treated group, compared

to the tumour tissue excised from mice treated by CNIE-NPs. This could be explained by the sustained release of R848 at the tumour site, causing the phenotypic reeducation of TAMs. Fourth, gene expression level of cellular immune related markers (IFN-g, TGF-b) and macrophage markers (IL-12, IL-10, Nos2 and Arg-1) were also evaluated by qPCR. As shown in Fig. 3k, the high expression level of IFN-γ and low expression level of TGF-b in the tumour tissue confirmed that a strong tumour-specific immune response had been elicited. Furthermore, the secretion of IL-12 and Nos2 was found to be significantly upregulated, while the secretion of IL-10 and Arg-1 was significantly down-regulated, indicating a significant phenotypic conversion of TAMs from M2 state to M1 state, with NIE-NPs treatment, but not CNIE-NPs treatment nor saline control.

Intrinsic anti-tumour immune efficacy of bispecific NIE

Therapeutic efficacy study of programmable bispecific NIE was performed in syngeneic orthotopic 4T1 breast cancer-bearing mice. Mice were randomly divided into six groups, each received a different treatment regimen: (1) Saline; (2) $(EK)_3$-KLVFFK(*Pa)*/$(EK)_3$-KLVFFK(*R848*); (3) *pro*LLP2A-KLVFFK(*R848*) (single monomer); (4) LXY30-KAAGGK(*Pa)*/*pro*LLP2A-KAAGGK(*R848*) (untransformable negative control CNIE-NPs); (5) LXY30-KLVFFK(*Pa)*/*pro*LLP2A-KLVFFK(*Pa)* (fibrillar-transformation but absence of R848); (6) LXY30-KLVFFK(*Pa)*/*pro*LLP2A-KLVFFK(*R848*). Regimen 6 is the complete NIE-NPs, containing all 4 critical components: LXY30, *pro*LLP2A, R848, and KLVFF, whereas regimen 2, 3, 4 or 5 all lack some components of NIE-NPs. When tumour volume reached about 50 mm^3, all treatment regimens were tail vein injected consecutively eight times q.o.d. (13 mg/kg each dose) and the mice were continuously observed for 21 days (Fig. 4a). As shown in Fig. 4b, regimens 2, 3 and 4 were inactive. Regimen 5 (fibrillar-transformation but no R848) demonstrated significant tumour suppression compared to group 2, 3 and 4. Regimen 6 (NIE-NPs) was found to be the most efficacious with significant tumour growth suppression (Fig. 4b) and prolonged survival (Fig. 4d), indicating the importance of combination T cells homing strategy and sustained release of TLR7/8 agonist. None of the mice in this therapeutic study showed any symptoms of dehydration nor significant body weight loss during the entire treatment period (Fig. 4c). The survival curves correlated well with tumour growth results. The mice treated by regimen 6 (NIE-NPs) achieved a longer median survival time (62 d) compared with other treatment groups (29, 32.5, 33.5, 33.5 and 39 d for regimen 1, 2, 3, 4, and 5, respectively).

To elucidate the mechanism of immunotherapeutic effects induced by bispecific NIE, we collected the tumour tissues and thoroughly evaluate the profile of tumour-infiltration immune cells *via* flow cytometry analysis (Supplementary Fig. 21). We found that among the six treatment regimens, NIE-NPs (regimen 6) was the most potent inducer for increase in cell numbers of the following cell populations: CD45+, T cells, macrophages, dendritic cells, neutrophiles, B cells and monocytes. Compared to saline control, NK cells and eosinophil cells numbers were also increased with NIE-NPs treatment, but regimens 4 and 5 were equally effective in increasing these cell populations. Additional analysis (Fig. 4e and Supplementary Fig. 22) showed that only the treatment regimens capable of *in situ* fibrillar transformation and LLP2A display (regimen 5 and 6) were able to greatly increase the frequency of $CD3^+$ and $CD8^+$ T cells within the tumours, particularly in combination with immune adjuvant R848 (regimen 6, NIE-NPs), which was

consistent with the observed strongest anti-tumour effects in NIE-NPs. The percentage of M1-phenotype macrophage in total macrophages was 60%, which was much higher than that of other control groups (Supplementary Fig. 23). Tumour sections (H&E) obtained from mice treated with NIE-NPs revealed a marked decrease in Ki-67 expression, an increase in $CD8^+$ T cells, and a decrease in Foxp3 (T_{reg} cells), compared with other control groups (Supplementary Fig. 24). There was an increase in CD68 and a decrease in CD163, indicating that the phenotype of macrophages was reversed after 8 doses of NIE-NPs. It is known that $CD8^+$ T cells secrete cytokines IFN-g and TNF-a to kill tumour cells.[15, 39] The expression levels of IFN-g and TNF-a in the tumour tissue were further evaluated by qPCR. As shown in Fig. 4f, treatment regimen 6 (NIE-NPs) was the most efficacious in restoring the immunoactive state of the tumour microenvironment, with the highest expression levels of IFN-g and TNF-a. In addition, NIE-NPs also significantly induced expression of IL-12, IL-6 and Nos2, and suppressed expression of TGF-b, IL-10 and Arg-1, leading to the suppression of the T_{reg} cells recruitment and reeducation of M2-like macrophages to M1 phenotype. To better clarify the contribution of CD8 T cell recruitment to the tumour in NIE-NPs immunotherapy, we performed an CD8 T cell depletion experiment with an antibody (Fig. 4g). Syngeneic orthotopic 4T1 breast cancer-bearing mice were randomly divided into three groups: (1) saline; (2) regimen 6 (NIE-NPs) plus anti-CD8; (3) regimen 6 (NIE-NPs). Anti-CD8 depletion antibody (i.p. injection) was given at an initial dose of 200 μg 3 days before treatment and then given four doses on day 1, 5, 9 and 13. When tumour volume reached about 100 mm^3, NIE-NPs were injected *via* tail vein consecutively eight times q.o.d. (13 mg/kg each dose) and the mice were continuously observed for 21 days. As expected, the therapeutic efficacy of NIE-NPs was greatly diminished in mice given CD8 T cell-depleting antibody (lesser tumour inhibition and shorter survival), confirming the importance of tumour homing of CD8 T cells in the effectiveness of NIE-NP immunotherapy.

Bispecific NIE enhances ICB therapy against breast cancer and lung cancer

Since the receptor-mediated bispecific NIE could significantly mount systemic anti-tumour response by facilitating T_{eff} cells homing and reprogramming of TME, we believe it could enhance the efficacy of ICB therapy. It is well known that tumour cells hijack PD-1 receptors of T cells by overexpression of PD-L1, which can activate PD-1, leading to inhibition of T cell proliferation, activation, cytokine production, altered metabolism and cytotoxic T lymphocytes killer functions, and eventual death of activated T cells. Clinically, antibodies targeting PD-1 or PD-L1 have been demonstrated to be able to reinvigorate the “exhausted” T cells in the TME. To demonstrate the therapeutic synergy between bispecific NIE and PD-1/PD-L1 ICB therapy, we randomized syngeneic orthotopic 4T1 breast cancer-bearing mice into four groups for anti-PD-1 Ab (anti-PD-1) therapy with or without additional nanoparticles: (1) anti-PD-1 alone; (2) regimen 4 (CNIE-NPs) plus anti-PD-1; (3) regimen 5 plus anti-PD-1; (4) regimen 6 (NIE-NPs) plus anti-PD-1. When tumour volume reached about 100 mm^3, nanoparticles were given i.v. injected on day 1 (13 mg/kg), and anti-PD-1 (200 mg/mouse) given i.p. on day 2. The same cycle was repeated on day 3, 5, 7, and 9 for a total of 5 cycles, and mice were observed continuously for 21 days (Fig. 5a). Not unexpectedly, anti-PD-1 alone and regimen 4 plus anti-PD-1 treatment were ineffective (Fig. 5b). In contrast, regimen 5 plus anti-PD-1 treatment did significantly suppress tumour growth, resulting in a

longer median survival, compared with 8 treatments of regimen 5 without anti-PD-1 as shown in Fig. 4b,d (49.5 d vs. 39 d); both of these treatments however were not able to completely eliminate the tumours. Most remarkably, mice treated with regimen 6 (NIE-NPs) plus anti-PD-1 resulted in gradual shrinkage and eventual complete elimination of tumours within 21 days, and without any sign of recurrence during the observation period of 90 days (Fig. 5c), validating the synergistic effects of our bispecific NIE with ICB therapy. In addition to i.v. administration, we have also investigated the therapeutic efficacy of NIE-NPs *via* intratumoural (i.t.) injection plus anti-PD-1 antibody given i.p. As shown in Fig. 5 and Supplementary Fig. 25, both administration routes for NIE-NPs (i.v. or i.t.) yielded excellent immunotherapeutic efficacy. However, regimen 4 (i.t.) plus anti-PD-1 and regimen 5 (i.t.) plus anti-PD-1 groups were still unable to eliminate the tumour after five cycles of treatment, while i.t. injection of regimen 6 (NIE-NPs) plus anti-PD-1 group eventually eliminated tumour and maintained 100% survival rate within 90 days.

Unlike traditional chemotherapy or targeted therapy in clinical oncology, immunotherapy can potentially induce an adaptive response with capacity for memory.[40, 41] Immune memory is crucial to achieving durable tumour responses and preventing recurrence. To assess whether the synergistic therapy of bispecific NIE plus anti-PD-1 Ab could induce an immune memory response, we re-challenged the “cured” mice from previous experiment (regimen 6 plus anti-PD-1 treatment, Fig. 5a-c) with 4T1 tumour cells on the opposite mammary fat pad on day 90; naive mice of the same age were used as a negative control (Fig. 5d). The tumour volume of all the naïve mice increased rapidly within 30 days (Fig. 5e). However, either no tumour growth or significant delay in tumour growth was observed in mice previously treated successfully with NIE-NPs plus anti-PD-1 (Fig. 5f), confirming the presence of an excellent immune memory response mounted by these previously treated mice. Survival curves of this experimental group correlated well with tumour growth results (Fig. 5g). All mice remained alive during the 60-day observation period (day 90-150). In addition, the serum levels of cytokines such as TNF-a and IFN-g in this experimental group were found to be much higher than those in the control same age naïve mice group after re-challenged with 4T1 tumour cells for 6 days (Fig. 5h,i). These results suggest that a durable and robust T cell memory response was generated by regimen 6 (NIE-NPs) plus anti-PD-1 given previously.

Although the up to 40% response rate of ICB therapy in non-small cell lung cancer (NSCLC) is considered a clinical breakthrough, the overall survival of patients remains only 15% at 5 years and declines to less than 2% in patients with metastatic disease.[42] We speculated that like 4T1 breast cancer model, NIE would also synergize ICB treatment of NSCLC. As expected, complete tumour regression and prolonged survival was obtained for the treatment of Lewis lung syngeneic subcutaneous murine tumour model using NIE-NPs plus anti-PD-1 (5 cycles, Fig 5j-l). No systemic toxicity and weight loss were detected.

Discussion

In spite of the clinical success of ICB therapy, only a fraction of cancer patients benefits from it. Defects in T_{eff} cells homing to the tumour sites is probably one of the main reasons why many patients remain refractory to such treatment.[6] Development of approaches to convert an immunologically “cold” tumour

to a “hot” tumour is undergoing intense investigation around the world. We believe the receptor-mediated bispecific NIE reported here can provide a relatively simple solution to this challenge. By incorporating pro-ligand LLP2A and R848 to the *in vivo* transformable nanofibrillar networks, we have already demonstrated in syngeneic 4T1 breast cancer and Lewis lung cancer model that this non-toxic treatment can (1) facilitate the homing of T-cells to the tumour sites, (2) promote retention of T-cells at close proximity to the tumour cells, and (3) provide sustained release of R848 at the TME, resulting in the reeducation of TAMs to M1 phenotype *in vivo*, significantly enhancing the efficacy of anti-PD1 antibody based ICB. We have also clarified the role of T-cell capturing ligand (LLP2A) and TLR7/8 immunoagonist (R848) in NIE-NPs, in chemokine secretion and T cells homing to the TME. As shown in Supplementary Fig. 26a, R848 (group ii) was more effective in inducing chemokine secretion than LLP2A ligand (group iii), but the population of CD8 T cells in group iii was slightly higher than that in group ii, and the ratio of CD8 to T_{reg} cells was also higher (Supplementary Fig. 26b). This suggested that LLP2A ligands played a significant role in capturing and retaining CD8 T cells at the TME, more so than R848. However, LLP2A or R848, each alone was found to be insufficient to induce a robust anti-tumour immune response. It is clear that group iv, with both LLP2A and R848, was needed to mount a robust anti-tumour immune response, resulting in higher level of chemokine expression, more CD8 T cells and less T_{reg} cells, when compared to either LLP2A or R848 alone.

To demonstrate that the receptor-mediated bispecific NIE not only works well in murine tumours but also human tumours, we used MCF-7 breast cancer and A549 lung cancer cell lines and human primary T cells to confirm the formation of nanofibrillar networks and capturing of human CD8 T-cells around these target tumour cells (Supplementary Fig. 27), indicating that the NIE strategy has great translational potential. Although NIE was found to be equally efficacious whether it was given i.t. or i.v. in 4T1 syngeneic tumour model with single subcutaneous tumour (Fig. 5 and Supplementary Fig. 25), i.t. administration is not as useful clinically since many patients do have multiple tumour lesions, many of which may not be easily accessible for i.t. injection. Because NIE is relatively non-toxic, intravenous administration is the preferred route, so that each and every tumour lesion will be treated and be converted from immunologically “cold” to “hot”.

Since the programmable bispecific NIE is modular, we have the options of combinatorially incorporating various different ligands, pro-ligands, or immunomodulators to generate a series of nano-engagers that may be applied for capturing other beneficial immune cells, including natural killer cells. Other potent immunomodulators against other pathways such as the stimulator of IFN genes (STING) pathway may also be tried. One unique feature of NIE therapy is that the nanofibrillar network formed at the TME is durable, which may explain its remarkable *in vivo* anti-tumour immune response and memory effects but without any sign of systemic immunotoxicity. This programmable bispecific NIE is highly robust. Each transformable peptide monomer is chemically well-defined, and the final immune-nanoparticle can be simply assembled from two or more monomers under aqueous condition. Scale-up production for clinical development should not be a problem. Work is currently undergoing in our laboratory on using other ligands and immunomodulators against other cancers besides breast and lung.

Methods

Preparation of transformable peptide monomers (TPMs). All TPMs were synthesized by standard solid-phase peptide synthesis techniques. LXY30-KLVFFK(Dde)-Beads, LXY30-KAAGGK(Dde)-Beads, LLP2A-KLVFFK(Dde)-Beads and LLP2A-KAAGGK(Dde)-Beads were firstly synthesized in sequence. Then amino protection group (Dde) was removed for 5 h using the mixed solution of imidazole and hydroxylamine (the ratio was 3:4). For LXY30-KLVFFK(NH_2)-Beads and LXY30-KAAGGK(NH_2)-Beads, pheophorbide a (*Pa*) as a hydrophobic unit was linked. For LLP2A-KLVFFK(NH_2)-Beads and LLP2A-KAAGGK(NH_2)-Beads, succinic anhydride and resiquimod (*R848*) were successively conjugated. Then these peptides were cut off from the beads for 3 h using the solution with 82.5% TFA, 5% DI water, 5% phenol, 5% thioanisole reagentplus, 2.5% triisopropylsilane. Cold ether was used to precipitate these peptide products. LXY30 ligands in LXY30-KLVFFK(*Pa*) and LXY30-KAAGGK(*Pa*) peptides were crosslinked *via* CLEAR-OX. In addition, 3-methoxy-1-propanol was used to block the carboxyl group in LLP2A ligands *via* ester bond. After cold ether precipitation, *pro*LLP2A-KLVFFK(*R848*) and *pro*LLP2A-KAAGGK(*R848*) peptides were eventually acquired. Finally, these peptides were purified by high performance liquid chromatography (HPLC, water 2998, US). The molecular weight of TPMs were confirmed by matrix-assisted laser desorption ionization time-off light mass spectrometer (MALDITOF mass spectra, Bruker Daltonics).

Self-assembly preparation and characterization of nanoparticles. TPMs were dissolved in DMSO to form a solution. Peptide solutions (LXY30-KLVFFK(*Pa*):*pro*LLP2A-KLVFFK(*R848*) is 1:1; 5 + 5 μL) was further diluted with DMSO (990, 790, 590, 390, 190, 90, 10 and 0 μL) and mixed with deionized water (0, 200, 400, 600, 800, 900, 980 and 990 μL). The ultraviolet-visible absorption (UV-vis) and fluorescence spectra (*ex*: 405 nm, UV-1800, Shimadzu and RF6000, Shimadzu) of solutions with varying water content were measured to validate the formation of nano-immuno-engager nanoparticles (NIE-NPs). The excitation and emission bandwidths were both set as 5.0 nm, and the data interval was 1 nm.

Fresh NIE-NPs, CNIE-NPs, NPs_{TPM1} and NPs_{TPM2} (99% water content, 20 μM) were used for measurement as an initial state. The morphology transformation of NIE-NPs to NIE-NFs was performed by the addition of $\alpha_3\beta_1$ integrin receptor protein or esterase plus $\alpha_4\beta_1$ integrin receptor protein (Sigma-Aldrich) and cultured for several hours at 37°C. The NIE-NP and NIE-NF solutions were used for size/zeta potential (DLS, Nano ZS), TEM measurement (CM-120 TEM, Phillips), circular dichroism (JASCO) and fluorescence spectra. TEM samples were dyed with uranyl acetate. Pyrene molecules were employed as an indicator to determine the CAC of nanoparticles, by comparing the fluorescence of their third and first emissive peaks. First, NIE-NPs or NIE-NFs was diluted to different concentrations (0.01, 0.05, 0.1, 0.5, 1, 5, 10, 20, 30 and 50 μM), then 999 μL of NIE-NPs or NIE-NFs of each dilution was incubated with 1 μL of pyrene acetone solution (0.1 mM) at 37°C for 2 h. The fluorescence spectra of pyrene (excitation, 335 nm) in different NIE-NPs or NIE-NFs dilutions were recorded. The fluorescence intensity ratio (I_3/I_1) of the third and first emissive peaks was measured for CAC calculation. Stability of NIE-NPs in the presence of human plasma and protease. The stability of NIE-NPs was studied in 10 % (v/v) plasma from healthy human volunteers

and protease solution. The mixture was incubated at physiological body temperature (37 °C) followed by size measurements at predetermined time intervals up to 168 h.

Accumulated drug release of R848 from NIE-NFs was triggered by acidic pH 6.5 and porcine liver esterase (100 U mL^{-1}). Considering the experimental design (R848 was released from NIE-NFs in the tumour microenvironment), we firstly prepared NIE-NP solution (100 μM), and then transformed into NIE-NFs after the interaction with $\alpha_3\beta_1$ integrin soluble protein. Then pH value in NIE-NF solution was set up to 6.5 and porcine liver esterase was added into NIE-NF solution. The mixture was incubated at 37 ^oC. At timed intervals, 20 μL solution was taken out and added into 80 μL DMSO for HPLC. Based on the pre-established calibration curves, free R848 concentration was calculated according to the integral area of free R848. Each value was reported as the means of the triplicate samples.

Cell line. The 4T1 breast cancer cell, Lewis lung cancer cell, MCF-7 breast cancer cell, A549 lung cancer cell, Jurkat cell and normal human peripheral blood mononuclear cell (PBMC, ATCC: PCS-800-011) were purchased from the American Type Culture Collection. Cell line authentication was performed by short tandem repeat DNA profiling. The cell line has been tested for mycoplasma contamination routinely. Cancer cell culture was performed in a cell incubator (5% carbon dioxide and 10% humidity. Temperature is 37°C). These cancer cells were cultured in RPMI-1640 medium with 10% FBS and antibiotics containing penicillin and streptomycin.

In vitro **cytotoxic assay.** 4T1 cells were used to evaluate the cytotoxicity of NIE-NPs and CNIE-NPs. Cells were seeded in 96-well plates (a density of 6000 cells per well, *n* = 3), cultured with RPMI-1640 and supplemented with 10% FBS and 1% penicillin at 37°C in a humidified environment containing 5% CO_2. A 1% DMSO solution was diluted by RPMI-1640 (0.5, 1, 5, 10, 20 and 50 μM) and then added to each well for incubation with cells. After 48 h of incubation, MTS reagent was added into each well. The relative cell viabilities were measured by Micro-plate reader (SpectraMax M3, USA). Percentage of cell viability represented drug effect, and 100% means all cells survived. Cell viability was calculated using the following equation: Cell viability (%) = (OD490nm of treatment/OD490nm of blank control) × 100%.

CLSM and SEM validation of structural transformation on living cell surface. 4T1 cells were cultured in glass-bottom dishes for 12 h until all cells were completely attached. NIE-NPs and CNIE-NPs (50 μM) were incubated with cells in RPMI-1640 at 37°C for different time, respectively. For confocal laser scanning microscopy imaging (CLSM 800, ZEISS), specimens were fixed with glutaraldehyde (4%) for 10 min, washed with PBS three times, and examined with a 63× immersion objective lens and a 405-nm laser. For SEM (Phillips XL30 TPM, FEI), cells were fixed with glutaraldehyde (4%) overnight and then coated with gold for 2 min. For stability of nanofibril on the cell surface experiment, 4T1 cells were firstly incubated with different NPs for 6 h, and the extra free NPs were removed. Then the cells continued to be incubated in the fresh medium without NPs for another 18 h. After that, specimens were fixed with glutaraldehyde (4%) for 10 min and washed with PBS three times for CLSM imaging. To simulate the processes of initial fibrillar transformation of NIE-NPs on the 4T1 cells surface followed by T cell homing, NIE-NPs was first incubated with 4T1 cells for 6 h, unbound NIE-NPs were then washed off, followed by addition of fresh

medium containing esterase but without NIE-NPs. After 1 h of incubation, Jurkat cells were added and incubated with 4T1 cells for 2 or 4 h. After that, unbound Jurkat cells were gently removed prior to CLSM imaging. Jurkat cells could be replaced by murine CD8 T cells. Similar experiment was performed using human CD8 T cells and human cancer cells (MCF-7 breast cancer cell and A549 lung cell).

The phenotype reeducation of tumour-associated macrophages. The bone marrow derived macrophage (BMDM) was firstly isolated, cultured and differentiated. In brief, femur and tibia bones from 6-8-week-old C57BL/6J mice were isolated, cleaned with PBS and cut open on both ends. Then a 21G needle and 10 ml syringe was used to flush out bone marrow into cold PBS plus 2% heat inactivated fetal bovine serum (FBS) (3-5 mL/mouse) and the marrow was allowed to pass through the needle 4-6 times to dissociate the cells. The bone marrow solution was then filtered through a 100 μm cell strainer to remove cell clumps, bone, hair and other cells/tissues. The collected cells mixture was mixed with 3 volume of RBC lysis buffer, and incubated on ice for 10min to remove red blood cells, followed by washing with PBS. The bone marrow cells were then cultured in BMDM growth medium (Iscove's Modified Dulbecco's Medium (IMDM) + 10% FBS + 10 ng/ml M-CSF) for 7 days to obtain mature macrophage cells. On day 7, for immune-suppressive M2-polarized phenotype activation, IMDM containing 10% FBS and 10 ng/mL IL-4 was added for 24 h; for anti-tumourigenic M1-polarized phenotype activation, R848 or NIE-NFs plus esterase, different incubation times were used.

Animal model. All animal experiments were performed in accordance with protocols No.19724, which was approved by the Animal Use and Care Administrative Advisory Committee at the University of California, Davis. The jugular vein of male Sprague-Dawley rats was cannulated, and a catheter was implanted for intravenous injection and blood collection (Harland, Indianapolis, IN, USA). NIE-NPs and CNIE-NPs (total 13 mg/kg) were i.v. administrated into rat (n = 3). Whole blood samples (~100 μL) were collected *via* jugular vein catheter before dosing and at predetermined time points post-injection. The whole blood samples were then centrifuged for serum collection, then the blood serum was diluted with DMSO (20 μL serum was added to 80 μL DMSO) for fluorescence measurements. The concentrations were measured by testing the fluorescence of *Pa* (Ex = 405 nm and Em = 675 nm). The values were calculated by molar concentration first, then exchanged to μg per mL. Female Balb/c mice were 6-8 weeks of age (weight 22 ± 2 g), which were purchased from Envigo. 4T1 cells (5×10^6 cells per mouse) were inoculated into the left mammary fat pad of each female Balb/c mice. After around 10 days, NIE-NPs and CNIE-NPs (total 13 mg/kg) were injected *via* the tail vein and *ex vivo* images of tumour, heart, liver, spleen, lung, kidney, intestine, muscle, skin were collected at 10, 24, 48, 72, 120 and 168 h post injection. The images were obtained by *in vivo* fluorescence imaging system (Carestream In-Vivo Imaging System FXPRO, USA). Tumours were excised and fixed with glutaraldehyde (4%) at 72 h post injection of NPs for TEM imaging.

Flow cytometry. To elucidate the mechanism of immunotherapeutic effects induced by bispecific NIE, the profile of tumour-infiltration immune cells was thoroughly evaluated in tumour tissues after treatment *via* flow cytometry analysis (CD45+, T cells, Macrophages, Dendritic cells, Neutrophiles, B cells and Monocytes, NK cells and Eosinophil). TILs were isolated by first digesting tumour tissue with collagenase

type IV (2.5 mg/ml, Gibco) for one hour and the content was harvested after passing through 70 μm filter. Cells were stained with the respective fluorochrome conjugated monoclonal antibodies to the cell surface markers as follows: anti-CD3 (145-2C11), anti-CD8 (53-6.7), anti-CD45 (30-F11), anti-CD4 (RM4-5), anti-Foxp3 (NRRF30). The fluorescence stained cells were analyzed with a LSRFortessa (BD) and FlowJo software v.10 (TreeStar). Gating was performed based on the justification of first gate, exclusion of doublets by SSC-W and SSC-H, exclusion of dead cells by selection of Zombie aqua (BioLegend)/$CD45^+$. $CD3^+$ T cells, $CD4^+$ T cells, $CD8^+$ T cells, T_{reg} from TIL suspensions were analyzed using FlowJo software v.10. The results were based on the percentage of positively stained cells relative to upper gate cell number.

In vivo **therapeutic effect.** Balb/c mice with 4T1 cells (5×10^6 cells per mouse) tumour inoculated into the left mammary fat pad were used in our experiments. The mice were randomly divided into six groups at 10 days post-tumour inoculation. Each of them treated with different regimen every 48 h *via* i.v. administration, and the total treatment was 8 injections (13 mg/kg each dose). During the process of the treatment (21 days), the tumour volumes and body weight were measured every three days. The survival data was recorded till all mice were dead. For the synergistic treatment between different regimen and anti-PD-1, Balb/c mice with 4T1 tumour were randomly divided into four groups at 10 days post-tumour inoculation. Each of them treated with different regimen on day 1 *via* i.v. administration, and then anti-PD-1 was given *via* i.p. injection. A total of five such cycles are performed. During the process of the treatment (21 days), the tumour volumes were measured every three days. The survival data was recorded till 90 days. For re-challenge tumour experiment, 4T1 cells (5×10^6 cells per mouse) were re-inoculated into the mice previously treated with NIE-NPs (regimen 6) plus anti-PD-1 Ab (200 μg each mouse) on day 90. Same age naïve mice were used as a control group. During the process of the treatment (30 days), the tumour volumes were measured every three days. The survival data was recorded till 60 days. Tumour tissues were collected for Haematoxylin and eosin (H&E), Ki-67, immunohistochemistry (IHC) staining, qPCR analysis and flow cytometric analysis images.

Statistical analysis.

Data are presented as the mean ± standard deviation (SD). The comparison between groups was analyzed with the student's *t*-test (two-tailed). The level of significance was defined at $*p < 0.05$, $**p < 0.01$ and $***p < 0.001$. All statistical tests were two-sided.

Declarations

Acknowledgements

This work was supported in part by NIH Grants R01CA115483, U01CA198880, R01CA247683, and R01EB012569 awarded to K.S.L.; R01CA232845 and R01DE029237 awarded to Y.L.; and National Key R&D Program of China (2018YFE0205400) awarded to L.W.

Author contributions

K.S.L. and L.Z. conceived the idea and developed the project. X.Y., K.E.L., K.L., Y.A., and R. L. assisted with the chemical synthesis and data analysis. R.B., W.X., T.R., Y.W., D.Z. and C.M.B assisted with the cell culture studies. R.B., Y.W., L.L., Z.Z., A.H.M., W.X., Y.H., H.Z. and D.J. assisted with the animal studies. L.W. and Y.L. assisted with the design and supervision of part of the project, and revision of the manuscript. K.S.L. and L.Z. co-wrote the paper and all authors commented on the manuscript. L.Z. conducted all experiments and analyzed the data. K.S.L. supervised the entire project.

Competing interests

The authors declare the following competing financial interest(s): K.S.L. and L.Z. are the co-inventors of a patent on the fibrillar transformable nanoparticles (PCT/US2020/046495). K.S.L. is the founding scientist of LamnoTherapeutics Inc. which plans to develop the nanotherapeutics described in the manuscript. The remaining authors declare no competing interests.

Additional information

Supplementary information is available.

References

1. Postow, M.A., Sidlow, R. & Hellmann, M.D. Immune-related adverse events associated with immune checkpoint blockade. *New. Engl. J. Med.* **378**, 158–168 (2018).
2. Topalian, S.L., Taube, J.M., Anders, R.A. & Pardoll, D.M. Mechanism-driven biomarkers to guide immune checkpoint blockade in cancer therapy. *Nat. Rev. Cancer* **16**, 275–287 (2016).
3. Vaddepally, R.K., Kharel, P., Pandey, R., Garje, R. & Chandra, A.B. Review of indications of FDA-approved immune checkpoint inhibitors per NCCN guidelines with the level of evidence. *Cancers* **12**, 738 (2020).
4. Ribas, A. & Wolchok, J.D. Cancer immunotherapy using checkpoint blockade. *Science* **359**, 1350–1355 (2018).
5. Gotwals, P. et al. Prospects for combining targeted and conventional cancer therapy with immunotherapy. *Nat. Rev. Cancer* **17**, 286–301 (2017).
6. Sackstein, R., Schatton, T. & Barthel, S.R. T-lymphocyte homing: an underappreciated yet critical hurdle for successful cancer immunotherapy. *Lab. Invest.* **97**, 669–697 (2017).
7. Fares, C.M., Allen, E.M.V., Drake, C.G., Allison, J.P. & Hu-Lieskovan, S. Mechanisms of resistance to immune checkpoint blockade: why does checkpoint inhibitor immunotherapy not work for all patients? *ASCO. Educational Book* **39**, 147–164 (2019).
8. Rodell, C.B. et al. TLR7/8-agonist-loaded nanoparticles promote the polarization of tumour-associated macrophages to enhance cancer immunotherapy. *Nat. Biomed. Eng.* **2**, 578–588 (2018).

9. Zhang, L. et al. Unique photochemo-immuno-nanoplatform against orthotopic xenograft oral cancer and metastatic syngeneic breast cancer. *Nano Lett.* **18**, 7092–7103 (2018).
10. Riley, R.S., June, C.H., Langer, R. & Mitchell, M.J. Delivery technologies for cancer immunotherapy. *Nat. Rev. Drug Discov.* **18**, 175–196 (2019).
11. Zhang, C. & Pu, K. Molecular and nanoengineering approaches towards activatable cancer immunotherapy. *Chem. Soc. Rev.* **49**, 4234–4253 (2020).
12. Shi, J., Kantoff, P.W., Wooster, R. & Farokhzad, O.C. Cancer nanomedicine: progress, challenges and opportunities. *Nat. Rev. Cancer* **17**, 20–37 (2017).
13. Nam, J. et al. Cancer nanomedicine for combination cancer immunotherapy. *Nat. Rev. Mater.* **4**, 398–414 (2019).
14. Jain, R.K. & Stylianopoulos, T. Delivering nanomedicine to solid tumours. *Nat. Rev. Clin. Oncol.* **7**, 653–664 (2010).
15. Xiao, Z. et al. Dual pH-sensitive nanodrug blocks PD-1 immune checkpoint and uses T cells to deliver NF-κB inhibitor for antitumour immunotherapy. *Sci. Adv.* **6**, eaay7785 (2020).
16. Zhang, L. et al. Transformable peptide nanoparticles arrest HER2 signalling and cause cancer cell death in vivo. *Nat. Nanotechnol.* **15**, 145–153 (2020).
17. Li, Y., Wang, Y., Huang, G. & Gao, J. Cooperativity principles in self-assembled nanomedicine. *Chem. Rev.* **118**, 5359–5391 (2018).
18. Wang, H., Feng, Z. & Xu, B. Assemblies of peptides in a complex environment and their applications. *Angew. Chem. Int. Ed.* **58**, 10423–10432 (2019).
19. Cheng, K. et al. Sequentially responsive therapeutic peptide assembling nanoparticles for dual-targeted cancer immunotherapy. *Nano Lett.* **18**, 3250–3258 (2018).
20. Yang, P.-P. et al. A biomimetic platelet based on assembling peptides initiates artificial coagulation. *Sci. Adv.* **6**, eaaz4107 (2020).
21. Luo, Q. et al. A self-destructive nanosweeper that captures and clears amyloid β-peptides. *Nat. Commun.* **9**, 1–12 (2018).
22. Xiao, W. et al. Discovery and characterization of a high-affinity and high-specificity peptide ligand LXY30 for in vivo targeting of α3 integrin-expressing human tumours. *Ejnmmi. Res.* **6**, 18 (2016).
23. Yang, P.P. et al. Host materials transformable in tumour microenvironment for homing theranostics. *Adv. Mater.* **29**, 1605869 (2017).
24. Tan, J. et al. Role of CD40 ligand in amyloidosis in transgenic Alzheimer's mice. *Nat. Neurosci.* **5**, 1288–1293 (2002).
25. Hock, C. et al. Generation of antibodies specific for β-amyloid by vaccination of patients with Alzheimer disease. *Nat. Med.* **8**, 1270–1275 (2002).
26. Peng, L. et al. Combinatorial chemistry identifies high-affinity peptidomimetics against $\alpha_4\beta_1$ integrin for in vivo tumour imaging. *Nat. Chem. Biol.* **2**, 381–389 (2006).

27. Wang, C. et al. *In situ* formed reactive oxygen species-responsive scaffold with gemcitabine and checkpoint inhibitor for combination therapy. *Sci. Transl. Med.* **10**, eaan3682 (2018).
28. Pardoll, D.M. The blockade of immune checkpoints in cancer immunotherapy. *Nat. Rev. Cancer* **12**, 252–264 (2012).
29. Sharma, P. & Allison, J.P. The future of immune checkpoint therapy. *Science* **348**, 56–61 (2015).
30. Keller, N. et al. Enforcing extended porphyrin J-aggregate stacking in covalent organic frameworks. *J. Am. Chem. Soc.* **140**, 16544–16552 (2018).
31. Cheng, M.H., Harmatys, K.M., Charron, D.M., Chen, J. & Zheng, G. Stable J-aggregation of an aza-BODIPY-lipid in a liposome for optical cancer imaging. *Angew. Chem. Int. Ed.* **131**, 13528–13533 (2019).
32. Maiti, N.C., Mazumdar, S. & Periasamy, N. J-and H-aggregates of porphyrin-surfactant complexes: time-resolved fluorescence and other spectroscopic studies. *J. Phys. Chem. B* **102**, 1528–1538 (1998).
33. Korevaar, P.A. et al. Pathway complexity in supramolecular polymerization. *Nature* **481**, 492–496 (2012).
34. Carney, R.P. et al. Targeting tumour-associated exosomes with integrin-binding peptides. *Adv. Biosyst.* **1**, 1600038 (2017).
35. Wang, F. et al. Supramolecular prodrug hydrogelator as an immune booster for checkpoint blocker-based immunotherapy. *Sci. Adv.* **6**, eaaz8985 (2020).
36. Park, C.G. et al. Extended release of perioperative immunotherapy prevents tumour recurrence and eliminates metastases. *Sci. Transl. Med.* **10**, eaar1916 (2018).
37. Lynn, G.M. et al. In vivo characterization of the physicochemical properties of polymer-linked TLR agonists that enhance vaccine immunogenicity. *Nat. Biotechnol.* **33**, 1201–1210 (2015).
38. Asselin-Paturel, C. et al. Type I interferon dependence of plasmacytoid dendritic cell activation and migration. *J. Exp. Med.* **201**, 1157–1167 (2005).
39. Grinberg-Bleyer, Y. et al. NF-κB c-Rel is crucial for the regulatory T cell immune checkpoint in cancer. *Cell* **170**, 1096–1108 (2017).
40. Schmid, D. et al. T cell-targeting nanoparticles focus delivery of immunotherapy to improve antitumour immunity. *Nat. Commun.* **8**, 1–12 (2017).
41. Gerlinger, M. et al. Intratumour heterogeneity and branched evolution revealed by multiregion sequencing. *N. Engl. J. Med.* **366**, 883–892 (2012).
42. Luo, Y.-H. et al. 5-year overall survival in patients with lung cancer eligible or ineligible for screening according to US Preventive Services Task Force criteria: a prospective, observational cohort study. *Lancet Oncol.* **20**, 1098–1108 (2019).

Figures

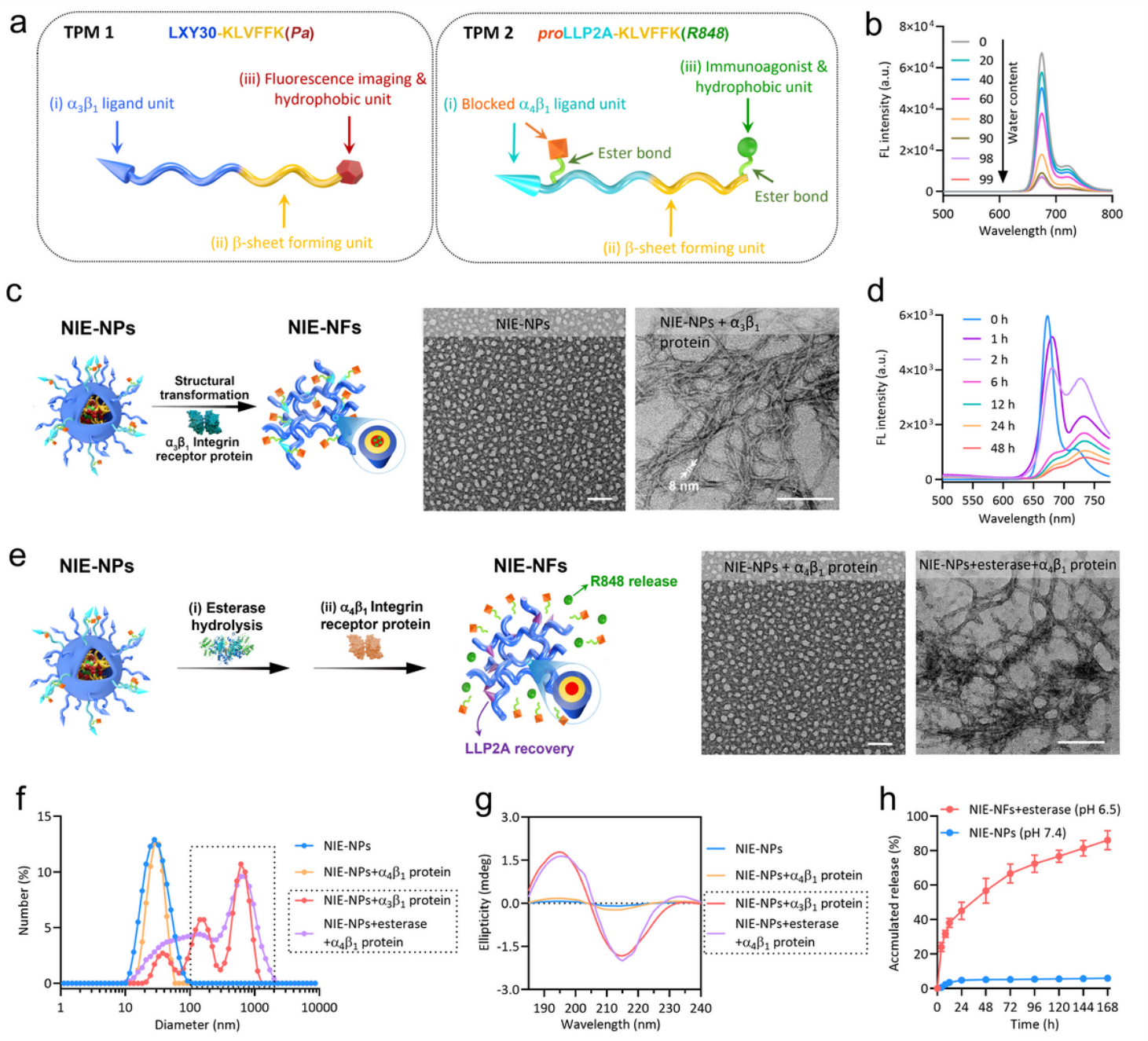

Figure 1

Assembly and fibrillar transformation of the programmable bispecific NIE, as well as esterase-induced LLP2A ligands exposure and R848 release. a, Schematic illustration of the molecular structure and function of TPM1 (LXY30-KLVFFK(Pa)) and TPM2 (proLLP2A-KLVFFK(R848)). b, Changes in fluorescence (FL) of DMSO solution of TPM1 and TPM2 at a 1:1 ratio following the gradual addition of water (from 0 to 99%) forming micellar NIE-NPs, excitation wavelength, 405 nm. Experiments were repeated three times. c, Schematic illustration and TEM images of initial NIE-NPs and subsequently transformed nanofibrils (NIE-NFs) upon interaction with soluble α3β1 integrin protein for 24 h (H2O to DMSO ratio of 99:1). The concentration of NIE-NPs used in the experiment was 20 μM. The scale bars in c are 100 nm. Experiments were repeated three times. d, Variation in fluorescence (FL) signal of Pa in the

fibrillar-transformation process of NIE-NPs to NIE-NFs over time. Experiments were repeated three times. e, Schematic illustration and TEM images of NIE-NPs upon interaction with soluble α4β1 integrin protein or α4β1 integrin protein plus esterase for 24 h (H2O to DMSO ratio of 99:1), respectively. The concentration of NIE-NPs used in the experiment was 20 μM. The scale bars in e are 100 nm. Experiments were repeated three times. f,g, Variation in size distribution (f) and circular dichroism spectra (g) of NIE-NPs and NIE-NFs under different conditions. Experiments were repeated three times. h, The in vitro release profile of R848 from NIE-NFs over time under different conditions. Data are presented as mean ± s.d., n = 3 independent experiments. The molar ratio of α3β1 or α4β1 integrin protein to peptide ligand was approximately 1:1000. a.u., arbitrary units; mdeg, millidegrees.

Figure 2

In vitro bispecific NIE binds both 4T1 breast cancer cells and Jurkat cells, and re-educates tumour-associated macrophages. a, Cellular fluorescence distribution images of NIE-NPs and CNIE-NPs interaction for 6 h with 4T1 tumour cells to show NIE-NPs around cells and CNIE-NPs inside cells. Scale bar in a is 10 μm. Experiments were repeated three times. b, Cellular fluorescence signal retention images of 4T1 tumour cells after exposure to NIE-NPs and CNIE-NPs for 6 h followed by incubation with fresh medium without nanoparticles for 18 h to show long-retention of NIE and short retention of CNIE. Scale bar in b is 10 μm. Experiments were repeated three times. c, Representative TEM images of 4T1 tumour cells treated with NIE-NPs and CNIE-NPs for 24 h, showing abundance of nanofibrils around cells treated with NIE-NPs. Scale bar in c is 200 nm. Experiments were repeated three times. The concentration of NIE-NPs was 50 μM. d, Cellular fluorescence distribution images of Jurkat T-lymphoma cells (GFP labeled) after incubation with esterase-pretreated NIE-NPs to show NIE around cells. Jurkat cells were used to mimic T-lymphocytes with high expression of α4β1 integrin. Scale bar in d is 10 μm. Experiments were repeated three times. e, Representative SEM images of untreated 4T1 tumour and Jurkat cells, 4T1 tumour cells treated with NIE-NPs and Jurkat cells treated with esterase-pretreated NIE-NPs for 6 h. Scale bar in e is 10 μm. Experiments were repeated three times. f, Experimental scheme and cellular fluorescence distribution images of NIE-NPs (fluorescent red), after interaction with 4T1 tumour and GFP-labeled Jurkat cells. It shows that nanofibrillar networks (bispecific NIE) covers 4T1 tumour cells, which in turn binds Jurkat T-cells. More incubation time, more bound Jurkat cells. Scale bar in f is 10 μm. Experiments were repeated three times. g, Representative SEM images of 4T1 tumour and Jurkat cells after treatment with NIE-NPs (see f). Experiments were repeated three times. h, Representative images of M2-like murine macrophages and subsequent reeducation by NIE-NFs, NIE-NFs plus esterase, or R848 at different time points. Scale bar in h is 20 μm. Experiments were repeated three times. Statistical significance was calculated using a two-sided unpaired t test; *P < 0.05, **P < 0.01, ***P < 0.001.

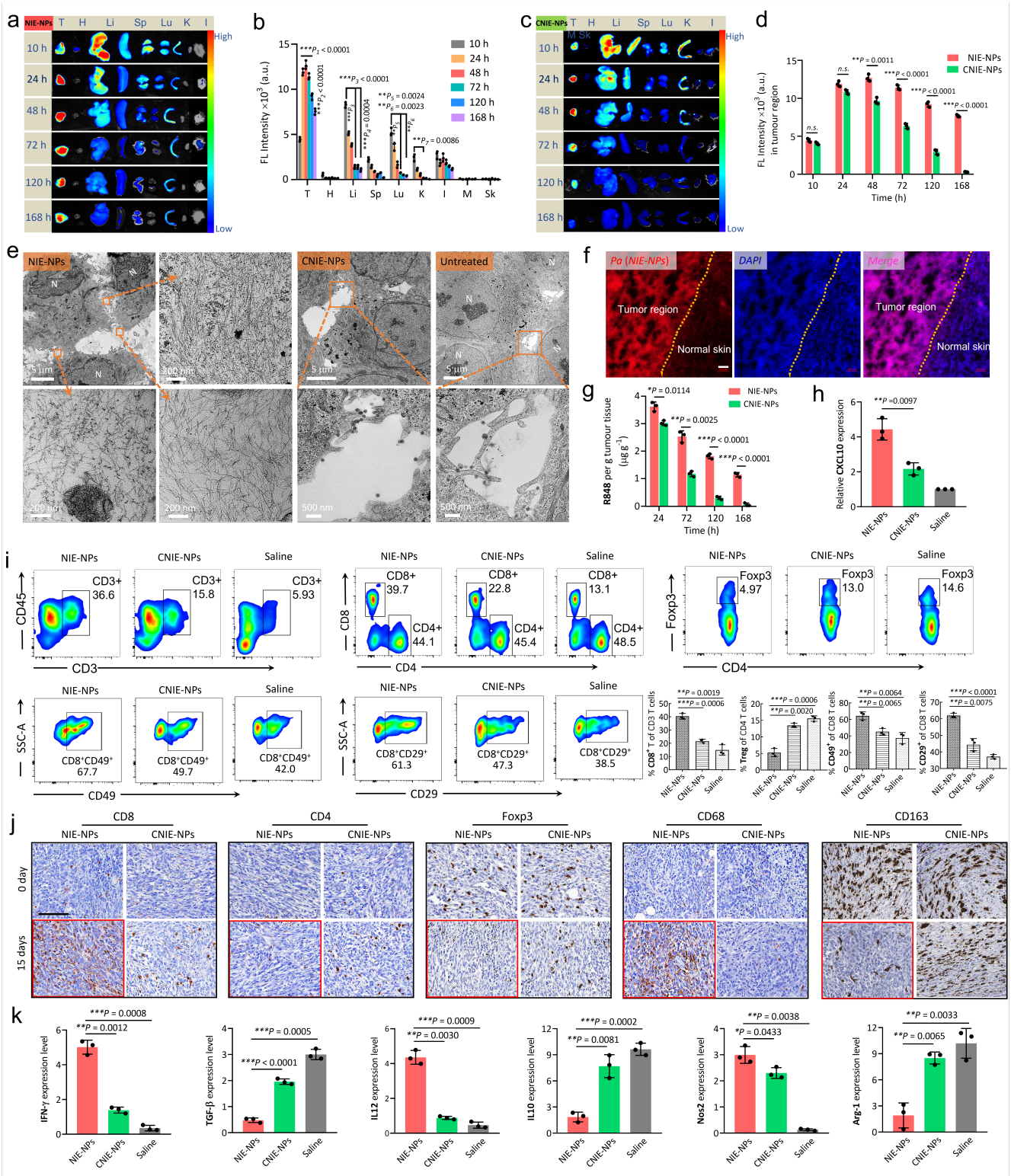

Figure 3

In vivo evaluation of NIE targeting tumour cells, and in situ nanofibrillar transformation to induce Teff cell homing and activate immunity. a,b, Time-dependent ex vivo fluorescence (FL) images (a) and quantitative analysis (b) of tumour tissues and major organs (heart (H), liver (Li), spleen (Sp), lung (Lu), kidney (K), intestine (I), muscle (M) and skin (Sk)) collected at 10, 24, 48, 72, 120 and 168 h post-injection of NIE-NPs. Data are presented as mean ± s.d., n = 3 independent experiments. c, Time-dependent ex vivo

fluorescence images of tumour tissues collected at 10, 24, 48, 72, 120 and 168 h post-injection of CNIE-NPs. Experiments were repeated three times. d, Fluorescence (FL) quantification of tumour tissues collected at 10, 24, 48, 72, 120 and 168 h post-injection of NIE-NPs and CNIE-NPs. Data are presented as mean ± s.d., n = 3 independent experiments. e, Representative TEM images of distribution in tumour tissue and in situ fibrillar transformation of NIE-NPs, CNIE-NPs and untreated control group at 72 h post-injection. “N” in e depicts nucleus. f, Fluorescence distribution images of NIE-NPs in tumour tissue region and normal skin tissue at 72 h post-injection (red, Pa of NIE-NPs; blue, DAPI; scale bars, 50 μm). g, R484 distribution retention in tumour tissues at different time points post injection of NIE-NPs and CNIE-NPs. Injection dose of R848: 0.94 mg kg−1; data were mean ± s.d., n = 3 for each time point. h, The expression of CXCL10 chemokine within the tumour tissues after 5 days of NIE-NPs, CNIE-NPs and saline treatment (n = 3; data were mean ± s.d.). i, Representative flow cytometric analysis images and corresponding quantification of CD45+CD3+, CD8+/CD4+, CD4+Foxp3+, CD8+CD49+, CD8+CD29+ T cell within the 4T1 tumours excised from mice treated with NIE-NPs, CNIE-NPs or saline control. j, Immunohistochemistry (IHC) of tumours excised from mice after treatment with NIE-NPs or CNIE-NPs. Representative images are shown for the IHC staining of T cells (CD8+, CD4+, Foxp3+) and macrophage markers (CD68, CD163). Scale bar in j is 100 μm. k, The expression levels (qPCR assay) of IFN-γ, TGF-β, IL12, IL10, Nos2 and Arg-1 in 4T1 tumours excised from mice 15 days after treatment with NIE-NPs or CNIE-NPs (n = 3; data were mean ± s.d.). Statistical significance was calculated using a two-sided unpaired t test compared to NIE-NPs group; *P < 0.05, **P < 0.01, ***P < 0.001.

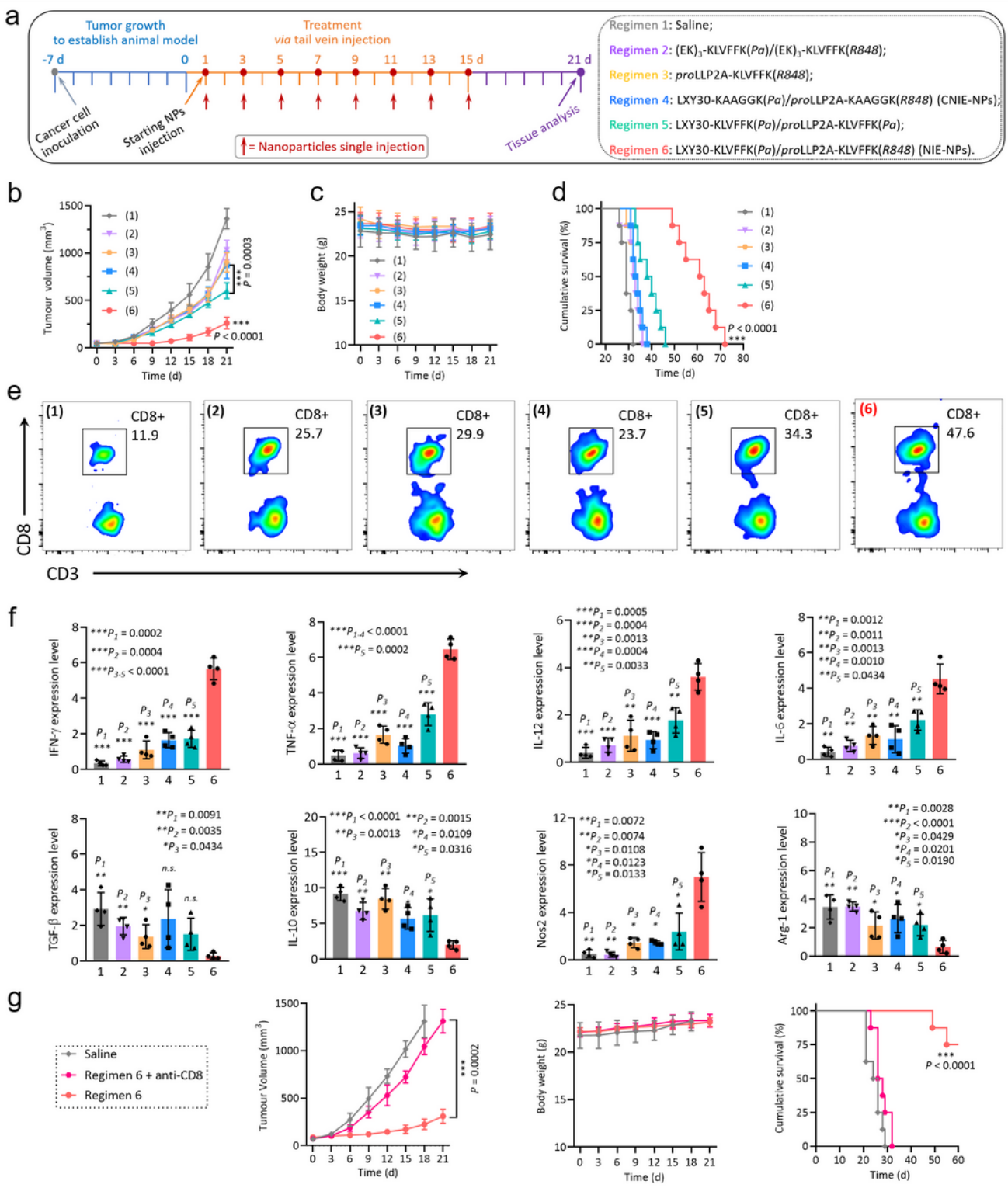

Figure 4

Intrinsic anti-tumour immune efficacy of bispecific NIE in Balb/c mice bearing 4T1 breast tumour. a, Experimental design: orthotopic tumour inoculation and treatment protocol; regimen 6 is NIE-NPs with all the 4 critical components. b,c, Observation of tumour inhibitory effect (b) and weight change (c) of mice bearing orthotopic 4T1 tumour over 21 d after initiation of treatment (n = 8 per group). Data are presented as mean ± s.d. d, Cumulative survival of different treatment groups of mice bearing 4T1 breast tumours.

e, Representative flow cytometric analysis images of CD3+CD8+ T cell within the 4T1 tumours excised from treated mice on day 21. f, The expression levels (analyzed by qPCR) of IFN-γ, TNF-α, IL12, IL6, TGF-β, IL10, Nos2 and Arg-1 in 4T1 tumours excised from mice on day 21 (data were mean ± s.d.). g, Observation of tumour growth inhibitory effect, weight change and cumulative survival of mice bearing orthotopic 4T1 tumour treated by regimen 6 plus anti-CD8 antibody (CD8 T cell depletion) and regimen 6 (n = 8 per group). Data are presented as mean ± s.d. Statistical significance was calculated using a two-sided unpaired t test compared to regimen 6; *P < 0.05, **P < 0.01, ***P < 0.001.

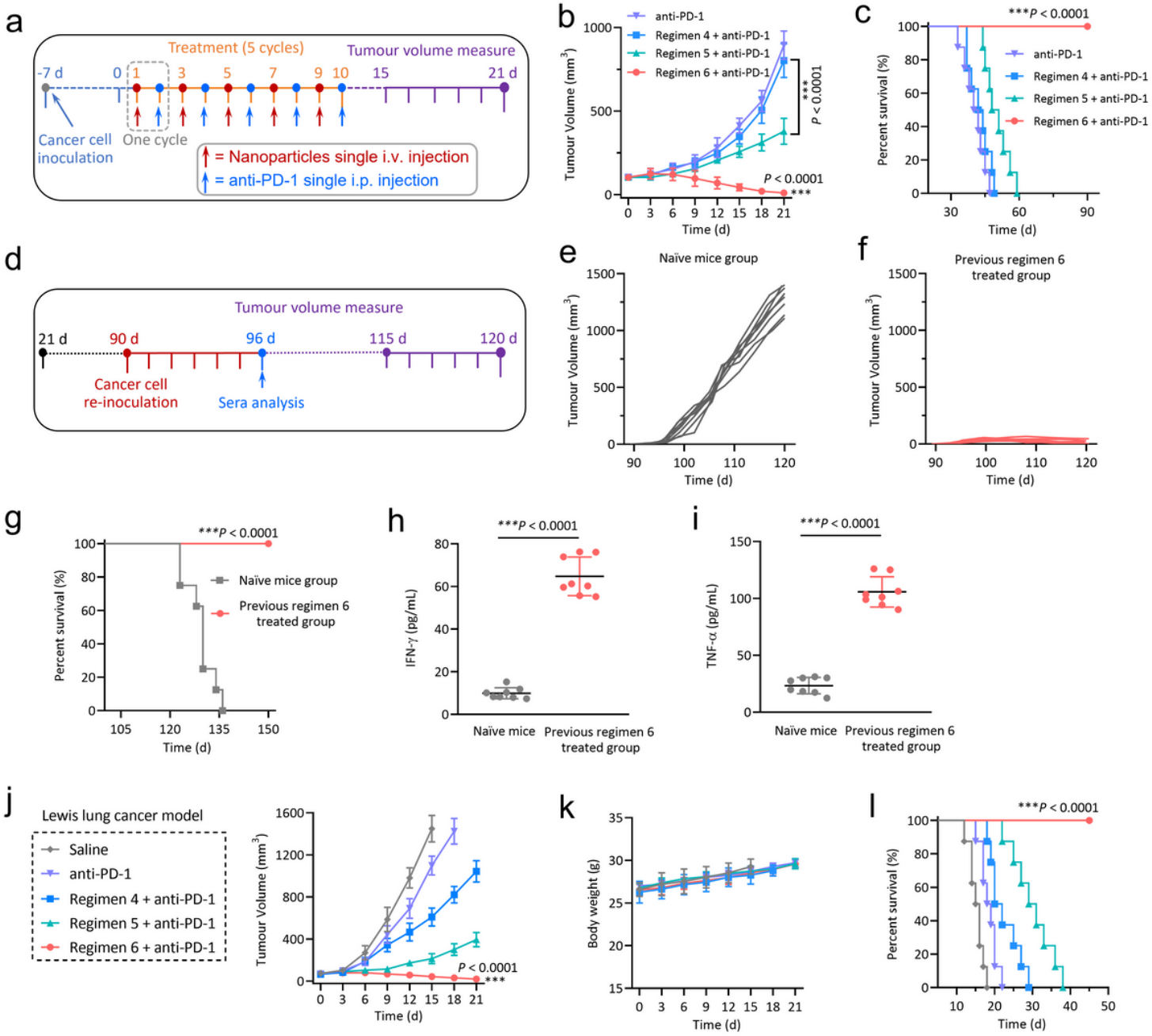

Figure 5

Bispecific NIE greatly enhances ICB therapy in mice bearing 4T1 breast tumour and Lewis lung tumour. a, Experimental design: orthotopic tumour inoculation and treatment protocol (4 treatment arms; regimens

4, 5 and 6 are the same as those shown in Fig. 4a). b, Tumour response in mice bearing orthotopic 4T1 tumour over 21 d of treatment (n = 8 per group). Data are presented as mean ± s.d. c, Cumulative survival of the four treatment groups. d, Experimental design: Mice previously treated with regimen 6 plus anti-PD-1 Ab were re-challenged with re-inoculation of 4T1 breast cancer cells on day 90. Same age naïve mice as a negative control group were carried out same operation. e, No anti-tumour immune memory effect was observed in same age naïve mice. f, Anti-tumour immune memory effect was observed in mice previously treated with regimen 6 and anti-PD-1 Ab. g, Cumulative survival of naïve mice and previously regimen 6 plus anti-PD-1 treated mice. h,i, IFN-γ (h) and TNF-α (i) level in mice sera 6 days after mice were re-challenged with 4T1 tumour cells. j,k, Observation of tumour inhibitory effect (j) and weight change (k) of mice bearing subcutaneous murine Lewis lung tumour over 21 d after initiation of treatment (n = 8 per group); Treatment protocol followed experiment design in a, 5 cycles (i.v. regimen 4-6 and i.p. anti-PD-1). Data are presented as mean ± s.d. l, Cumulative survival of different treatment groups of mice bearing subcutaneous murine Lewis lung tumours. Statistical significance was calculated using a two-sided unpaired t test; *P < 0.05, **P < 0.01, ***P < 0.001.

Supplementary Files

This is a list of supplementary files associated with this preprint. Click to download.

- SupplementaryInformation.pdf
- floatimage1.jpeg